Supramolecular association in the triclinic (Z′ = 1) and monoclinic (Z′ = 4) polymorphs of 4-(4-acetylphenyl)piperazin-1-ium 2-amino-4-nitrobenzoate

Mukesh M. Jotani,[I] James L. Wardell[II,III] and Edward R. T. Tiekink[*,IV]

[I] Department of Physics, Bhavan's Sheth R. A. College of Science, Ahmedabad, Gujarat 380001, India

[II] Fundação Oswaldo Cruz, Instituto de Tecnologia em FármacosFar Manguinhos, 21041-250, Rio de Janeiro, RJ, Brazil

[III] Department of Chemistry, University of Aberdeen, Old Aberdeen AB24 3UE, Scotland

[IV] Research Centre for Crystalline Materials, School of Science and Technology, Sunway University, 47500 Bandar Sunway, Selangor Darul Ehsan, Malaysia

Received; accepted

Keywords: Polymorphism / structures with Z' > 1 / carboxylate / Hirshfeld surface analysis / crystal structure analysis / X-ray diffraction

Abstract. Crystallography reveals two polymorphs for the salt [4-(4-acetylphenyl)piperazin-1-ium][2-amino-4-nitrobenzoate], a monoclinic form (**2**; modelled as $P2_1/n$ with Z' = 4) formed directly from the reaction mixture, and a triclinic form (**1**; Z' = 1) isolated from recrystallisation. Relatively minor differences are noted in the conformations of the anions and of the cations, mainly relating to the twist of, respectively, the carboxylate groups and piperazin-1-ium rings with respect to the phenyl rings they are connected to. The key feature of the packing of both forms is the formation of charge-assisted ammonium-N–H···O(carboxylate) hydrogen bonds which lead to cyclic 12-membered {···HNH···OCO}$_2$ synthons in the case of **1** but, supramolecular chains in **2**. The three-dimensional architecture in the crystal of **1** is further stabilised by amine-N–H···O(nitro) and amine-N–H···O(acetyl) hydrogen bonds, leading to double-layers in the bc-plane, which are linked along the a-axis by methylene-C10–H···O(carboxylate) and π-stacking interactions. The combination of ammonium-N–H···O(carboxylate) and amine-N–H···O(carboxylate, acetyl) hydrogen bonds consolidate the three-dimensional packing in the crystal of **2**. The greater crystal density, packing efficiency and calculated lattice energy for **1** compared with **2**, suggest the former to be the thermodynamically most stable crystal. An analysis of the Hirshfeld surfaces for **1** and **2** reveal distinctive features that differentiate between the constituents of the two forms and between the ions comprising the asymmetric unit of **2**.

[*] Correspondence author: edwardt@sunway.edu.my (E.R.T.T.)

Introduction

The first crystallographic investigations of the relatively simple carboxylic acid derivative, 2-amino-4-nitrobenzoic acid (or 4-nitroanthranilic acid), Figure 1a, were only reported at the beginning of the Century and since then there have only been 18 additional structures reported in the literature containing the acid or anions derived from this. This lack of investigation probably masks the inherent crystallographic interest in this compounds as evidenced by four fully characterised polymorphs of the acid [1,2]. Further, the neutral molecule has been characterised in two co-crystals, namely of 2,2′-bipyridine (1:0.5) and bis(pyridin-2-yl)methanone (1:1) [1]. The remaining structures features the anionic form, i.e. 2-amino-4-nitrobenzoate. Thus, the sodium dihydrate [3], potassium hydrate [3], rubidium hydrate [4] and caesium dihydrate [5] with higher coordination numbers for the larger alkali cations being achieved through bridging water molecules and the increased participation of nitro-O atoms in coordination. The remaining structures, namely of ammonium salts, often feature extensive hydrogen bonding interactions: ammonium hydrate [6], dimethyl- and di-*n*-butyl-ammonium [7], di-cyclohexylammonium [8], hydrazinium [9], morpholin-4-ium [10], guanidinium hydrate [11] as well as an example of a diammonium salt, namely ethylenediammonium, characterised as a dihydrate [12]. The only example of a metal complex with the anion is that of a binary lead(II) species [13]. It was during on-going investigations in this area [1,2,7.9] that the title polymorphic salts were isolated. The interest in the new structures arises not only as they are polymorphs, crystallising in triclinic and monoclinic forms, but because the latter also features four independent cation-anion pairs in the asymmetric unit, Figure 1b.

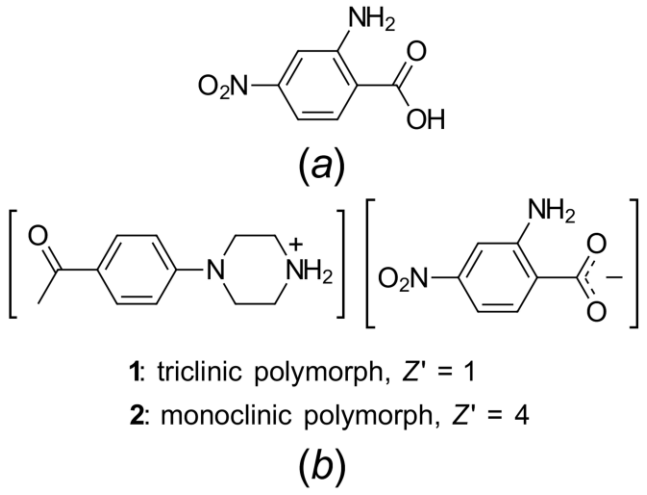

Fig. 1: Chemical structural formulae of (**a**) 2-amino-4-nitrobenzoic acid and (**b**) summary of the triclinic (**1**) and monoclinic (**2**) polymorphs for the salt, [4-(4-acetylphenyl)piperazin-1-ium][2-amino-4-nitrobenzoate].

Polymorphism continues to attract immense interest in the crystallographic community owing to the fundamental importance of the phenomenon itself, but because it has implications in materials chemistry and in the pharmaceutical industry [14]. This is because the crystal structure/molecular packing of a molecular compound can influence its physical and chemical properties, certainly as they relate to the solid-state owing to different packing arrangements. Computational chemistry suggests that many 10's, or even more, equally stable, at least to within a few kJ/mol, molecular packing arrangements may be found for organic molecules [15]. A search

of the Cambridge Structural Database (CSD) [16] for the term "polymorph" showed just over 3% of the structures included there were classified as such. Another estimate for the percentage of polymorphic compounds but for organic molecules only, again based on a search of the CSD, suggested less than 4% [17] with the low number of observations probably reflecting the lack of (systematic) screening – many (most) structural studies are directed towards establishing the molecular structure/chemical connectivity rather than exploring the potential for polymorph formation. Thus, it is of considerable interest that the numbers/percentage of polymorphic compounds increases significantly, to almost 50%, for systems that are systematically investigated for polymorphism, e.g. drugs/drug candidate molecules [14]. The thoughts of McCrone come to mind here where, paraphrasing, it was suggested the number of polymorphs revealed for a compound was proportional to the effort spent (and expenditure) in actually seeking polymorphs [18]. A recent and highly relevant exemplar of this concept is found in the 1:1 pharmaceutical co-crystal formed between carbamazepine:saccharin – after it was claimed that no new polymorphs would be found for this extensively studied system [19], a new polymorph was revealed, admittedly isolated under rather unusual conditions, i.e. having heteronuclei fashioned from functionalised cross-linked polymers [20]. In a related phenomenon to polymorphism, different packing arrangements for individual molecules also occur in crystals whereby multiple molecules comprise the crystallographic asymmetric unit, i.e. generally in circumstances with $Z' > 1$.

Debate on the reasons why crystals form with $Z' > 1$ continues and a recent review noted that approximately 9% of structures included in the CSD exhibited this feature [21]. The percentage of crystals with increasing numbers of molecules in the asymmetric unit rapidly drops off with only 284 organic structures having $Z' > 4$ [22]. Possible explanations behind such behaviour range from the idea that crystals with higher than usual values of Z are "fossil relics", being precursor (metastable) crystals to the more stable form, i.e. a snapshot of the crystallisation pathway, or more formally, are an isolated kinetic form rather than the final thermodynamic form [21-25]. It is also argued that some molecules, owing to size, shape and propensity to form specific intermolecular interactions can not be accommodated in the symmetry imposed by space groups, an argument famously proffered by Brock and Dunitz in the case of the rationalising the packing of alcohol derivatives in the crystalline state [26]; this behaviour has been labelled "synthon frustration" [27].

In instances of polymorphism and crystals with multiple molecules in the asymmetric unit, an analysis of intermolecular interactions can provide clues as to why either phenomenon occurs. An analysis of point to point interactions operating in a crystal structure can be analysed conveniently by geometric programs such as PLATON [28]. This type of examination can be enhanced by an analysis of the calculated Hirshfeld surfaces [29] through Crystal Explorer [30]. Here, the contact distances d_i and d_e from the Hirshfeld surface to the nearest atom inside and outside the surface, respectively, are calculated to enable the analysis of the intermolecular interactions. Crucially, the combination of d_e and d_i in the form of two-dimensional fingerprint plots [31] provides both a useful summary and convenient visualisation of the most prominent intermolecular contacts operating in a crystal. Importantly, these can be calculated for the entire crystal, encompassing all surface contacts, or for individual interactions, e.g. O–H···O contacts. The latter makes for facile but, detailed comparison between molecules in polymorphs and between multiple molecules in an asymmetric unit. Herein, the crystal and molecular structures of a monoclinic form of the title salt, isolated from the mother liquor, with $Z' = 4$ (**2**) are described along with those of a triclinic form with $Z' = 1$ (**1**) which was

isolated from a subsequent crystallisation. The structural study is augmented by an analysis of the calculated Hirshfeld surfaces of **1** and **2**.

Experimental

Synthesis and crystal growth

Solutions of 2-amino-4-nitrobenzoic acid (1 mmol) in MeOH (10 ml) and 1-(4-piperazin-1-ylphenyl)ethanone (1 mmol) in MeOH (15 ml) were mixed and heated under reflux for 30 min. The reaction mixture was left at room temperature for three days and the crystals which formed were collected and found to be the monoclinic polymorph (**2**). M.pt: 446 K (dec.).

Some crystals obtained as above were re-dissolved in ethyl acetate and left to stand at room temperature. After one week, crystals were harvested and found to be triclinic (**1**). M.pt: 443–446 K (dec.).

Crystal structure determination

Intensity data for **1** and **2** were measured at 100 K on a Rigaku Saturn724+ diffractometer using graphite-monochromatised MoKα radiation (λ = 0.71073 Å). Data processing and absorption corrections (ψ-scans) were accomplished with CrystalClear [32]. Unit cell data, X-ray data collection parameters and details of the structure refinement are given in Table 1. The structures were solved by Direct Methods using SHELXS [33] and full-matrix least-squares [34] refinement was on F^2 (anisotropic displacement parameters and C-bound H atoms in their idealised positions). The N-bound atoms were located from difference Fourier maps and were refined with the distance constraint 0.88±0.01 Å, and with U_{iso}(H) = U_{eq}(N). A weighting scheme of the form $w = 1/[\sigma^2(F_o^2) + (aP)^2 + bP]$ where $P = (F_o^2 + 2F_c^2)/3$ was introduced in each case. In the refinement of **1**, owing to poor agreement, the (1 2 2) reflection was omitted from the final cycles of refinement. The crystal of **2** employed for the analysis was not optimal as reflected in the high value of R_{int} = 0.169 and proved to be a challenging refinement of over 1000 parameters. There was no evidence of twinning. One the expert reviewers indicated the possibility of a lower symmetry space group for a twinned sample. One possibility could be $P2_1$ with Z' = 8, as there was some evidence for some *h* 0 *l* reflections being present/marginally above the background. However, based on the principle that the higher symmetry space group consistent with systematic extinctions is preferred, the $P2_1/n$ space group was selected for the analysis. In this model, there were no abnormal, non-systematic variations in geometric parameters, displacement parameters nor any evidence of disorder. Nevertheless, the structure has been determined unambiguously. Owing to poor agreement, a total of 17 reflections were omitted from the final refinement; these are listed in the deposited CIF. The programs WinGX [35], PLATON [28], ORTEP-3 for Windows [35], DIAMOND [36] and QMol [37] were also used in the study.

Tab: 1. Crystallographic data and refinement details for **1** and **2**.[1]

	1	**2**
Formula	$C_{12}H_{17}N_2O$, $C_7H_5N_2O_4$	$C_{12}H_{17}N_2O$, $C_7H_5N_2O_4$
Formula weight	386.40	386.40
Crystal colour, habit	Orange, blade	Orange, slab
Crystal size/mm	0.03 x 0.11 x 0.17	0.08 x 0.16 x 0.18
Crystal system	triclinic	monoclinic
Space group	$P\bar{1}$	$P2_1/n$

a/Å	7.1894(5)	12.466(2)
b/Å	10.7454(8)	22.524(3)
c/Å	12.4683(9)	26.611(4)
α/°	77.354(9)	90
β/°	75.166(9)	103.451(4)
γ/°	75.391(9)	90
V/Å^3	888.66(13)	7267.0(19)
Z/Z'	2/1	16/4
D_c/g cm^{-3}	1.444	1.413
F(000)	408	3264
μ(Mo$K\alpha$)/mm^{-1}	0.106	0.104
Measured data	11877	39350
θ range/°	2.4-27.5	2.2-25.0
Unique data	4031	12658
R_{int}	0.041	0.169
Observed data ($I \geq 2.0\sigma(I$	3493	9820
R, obs. data; all data	0.039; 0.110	0.124; 0.389
a, b in wghting scheme	0.065; 0.160	0.192; 54.035
R_w, obs. data; all data	0.045, 0.115	0.143; 0.401
$\Delta\rho_{max,\ min}$/e Å^{-3}	0.40, -0.19	0.63, 0.57

[1] Supplementary Material: Crystallographic data for the structures reported in this paper have been deposited with the Cambridge Crystallographic Data Centre as supplementary publication no. CCDC-1845456 and 1845457. Copies of available material can be obtained free of charge, on application to CCDC, 12 Union Road, Cambridge CB2 1EZ, UK, (fax: +44-(0)1223-336033 or e-mail: deposit@ccdc.cam.ac.uk).

Results

Experimental molecular structures

The asymmetric unit of the triclinic polymorph, **1**, comprises a single cation and a single anion, and that of the monoclinic polymorph, **2**, modelled in $P2_1/n$ (see Experimental), comprises four independent cation/anion-pairs. The molecular structures of the anions in **1** and **2** are shown in Figure 2a-e and those for the cations in Figure 3a-e. The confirmation of the deprotonation of the acid and protonation of the base is seen in distinct features of the structures, namely in the pattern of hydrogen bonding interactions (vide infra) and in the near equivalence of the C–O(carboxylate) bond lengths in the anions; both features are detailed below. For ease of comparison, the molecular structures of the anions in **1** and **2** will be described first, followed by a description of the cations.

The molecular structure of the anion in **1** is shown in Figure 2a. The transfer of a proton during recrystallisation of dimethylamine and 2-amino-4-nitrobenzoic acid is evidenced in the similarity of the C–O bond lengths [C7–O1, O2 = 1.2645(14) and 1.2623(14) Å]; key bond lengths and dihedral angles for **1** and **2** are collated in Table 2. Twists are apparent in the anion, in particular between the central phenyl ring and the carboxylate residue as seen in the dihedral angle of 21.22(4)º between the latter. Despite there being a twist between these residues, there is an intramolecular amine-N–H···O(carboxylate) hydrogen bond, Table 3. A far smaller twist is seen for the nitro group with the dihedral angle between it and the phenyl ring being 2.95(2)º. The dihedral angle between the carboxylate and nitro substituents is 23.52(7)º, consistent with a conrotatory relationship. To a

first approximation the cation in **1** is planar, allowing for the chair conformation of the piperazin-1-ium ring, Figure 3a. Thus, the dihedral angle between the acetyl group and phenyl ring is 7.66(4)° indicating a small twist. A small twist is also evident between the phenyl ring and the least-squares plane through the piperazin-1-ium ring as seen in the dihedral angle of 6.72(2)°; the dihedral angle between the outer planes is 1.53(5)°.

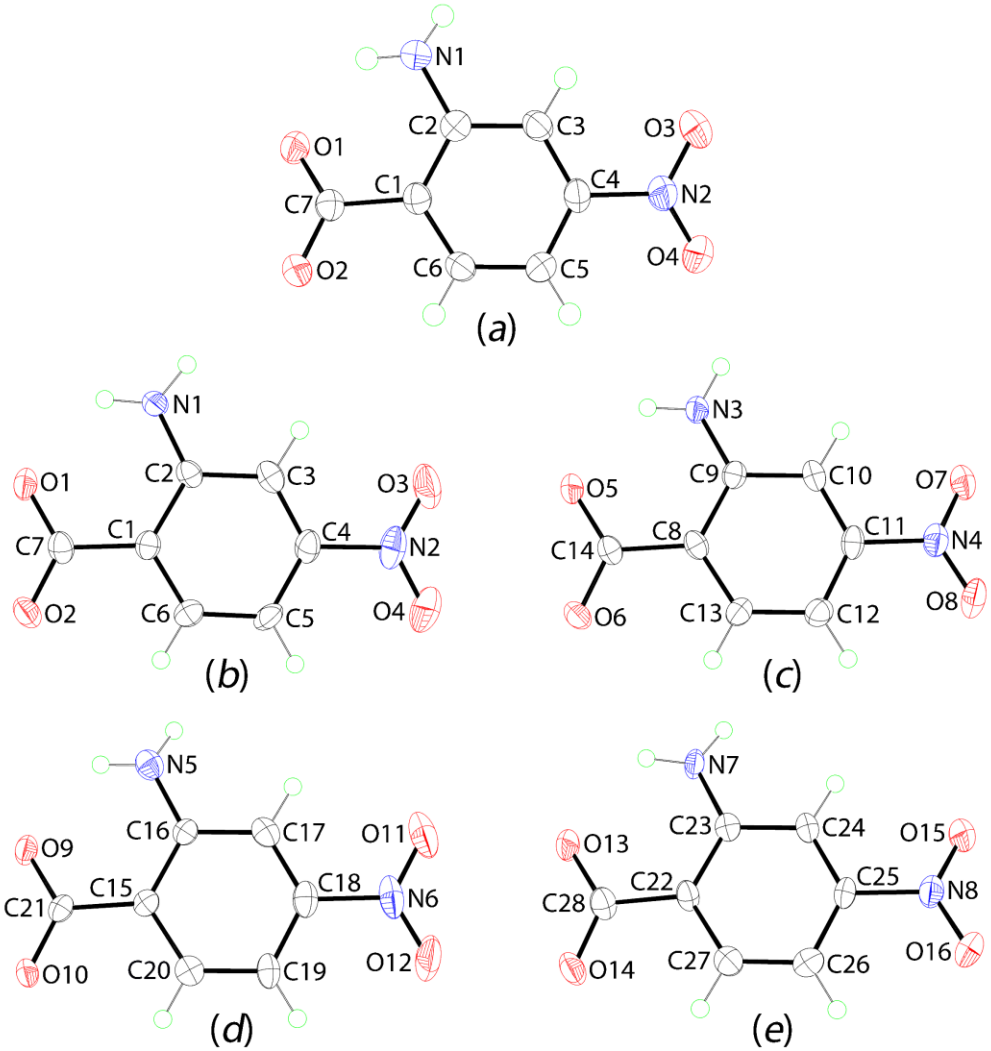

Fig. 2: The molecular structures of the anions in (**a**) **1** and (**b**)–(**e**) in **2**, showing the atom-labelling schemes and displacement ellipsoids at the 50% probability level.

Tab. 2: Summary of key geometric parameters (Å, º) for **1** and **2**.

Anions	**1**	**2**-O1	**2**-O5	**2**-O9	**2**-O13
C–O	1.2645(14), 1.2623(14)	1.267(8), 1.262(8)	1.275(8), 1.258(8)	1.263(8), 1.266(8)	1.274(8), 1.261(8)
C_6/CO_2	21.22(4)	6.5(2)	0.9(3)	7.2(2)	5.3(5)
C_6/NO_2	2.95(2)	2.5(3)	9.7(4)	2.7(3)	9.4(6)
CO_2/NO_2	23.52(7)	4.8(4)	10.3(4)	5.4(4)	14.6(6)
Cations	**1**	**2**-N10	**2**-N12	**2**-N14	**2**-N16
$C(=O)Me/C_6$	7.66(4)	3.7(5)	3.8(4)	7.85(17)	5.7(3)
C_6/C_4N_2	6.72(2)	7.5(4)	11.5(3)	5.97(11)	11.9(2)
$C(=O)Me/C_4N_2$	1.53(5)	7.7(5)	14.8(4)	13.82(17)	6.2(3)

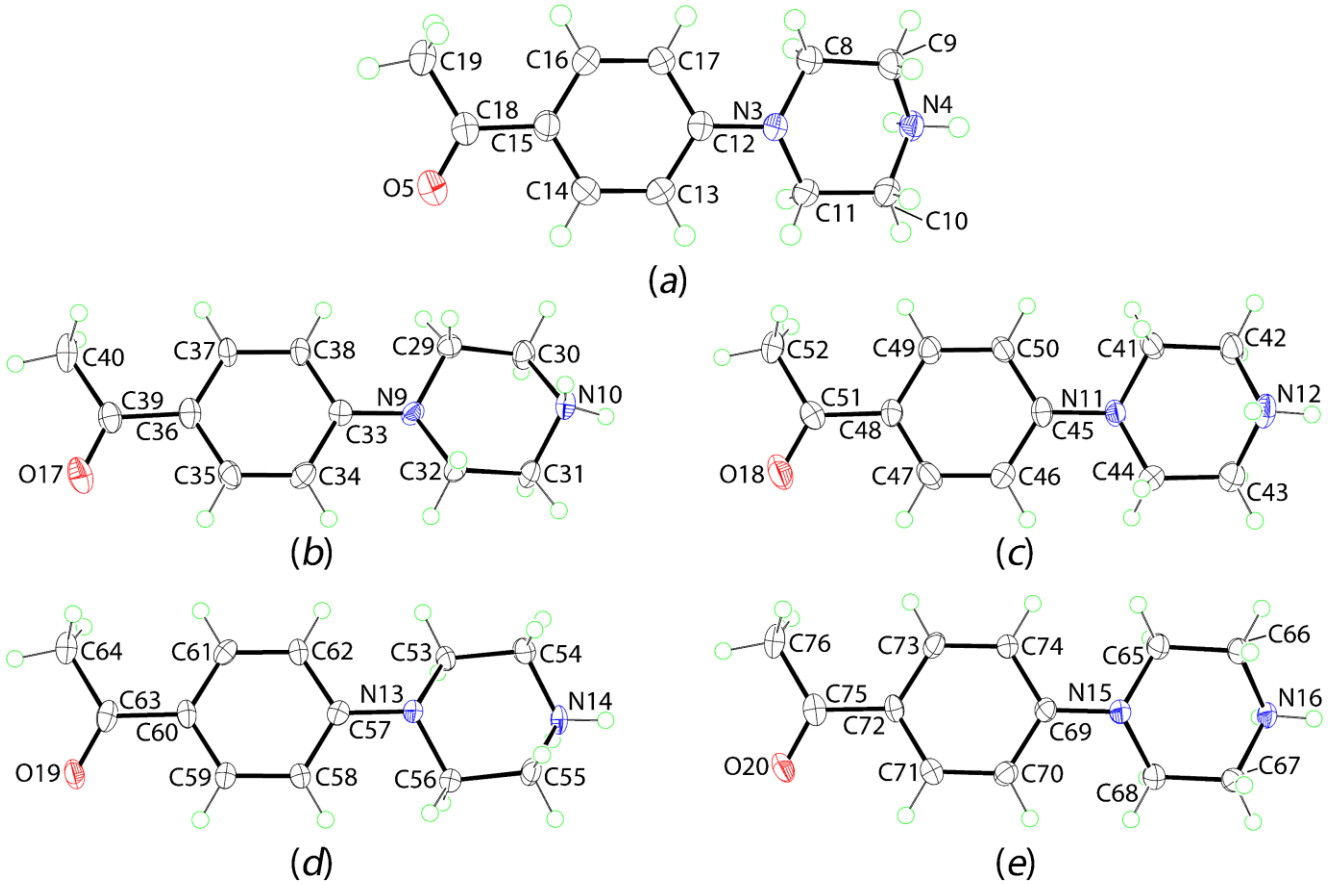

Fig. 3: The molecular structures of the cations in (**a**) **1** and (**b**)–(**e**) in **2**, showing the atom-labelling schemes and displacement ellipsoids at the 50% probability level.

Tab. 3: Summary of intra- and inter-molecular A–H···B and π···π interactions (Å, º) in the crystals of **1** and **2**.

A	H	B	A–H···B	H···B	A···B	A–H…B	Symmetry operation
1							
N1	H1n	O1	0.884(12)	2.037(13)	2.7274(14)	134.1(10)	x, y, z
N1	H1n	O5	0.884(12)	2.517(11)	3.2678(15)	143.2(11)	1+x, -1+y, z
N1	H2n	O3	0.889(12)	2.262(13)	3.1072(16)	158.6(12)	2-x, 1-y, 1-z
N4	H3n	O2	0.906(11)	1.846(11)	2.7474(13)	172.9(13)	1-x, -y, 2-z
N4	H4n	O1	0.895(12)	1.919(12)	2.7918(15)	164.5(13)	-1+x, y, z
C9	H9a	O5	0.99	2.58	3.2070(17)	121	x, -1+y, z
C10	H10a	O2	0.99	2.41	3.2697(16)	145	x, y, z
C10	H10b	O1	0.99	2.36	3.0490(15)	126	1-x, -y, 2-z
(C1-C6)	–	(C12-C17)	–	-	3.6644(8)	1.46(6)	x, y, z
2							
N1	H1n	O1	0.88(2)	2.02(6)	2.653(7)	128(6)	x, y, z
N3	H4n	O5	0.88(3)	1.97(6)	2.624(7)	130(6)	x, y, z
N5	H5n	O9	0.89(3)	2.01(7)	2.650(8)	129(6)	x, y, z
N7	H7n	O13	0.879(15)	2.11(6)	2.694(7)	124(6)	x, y, z
N1	H2n	O10	0.88(5)	2.08(5)	2.947(7)	168(5)	-x, 1-y, 1-z
N3	H3n	O17	0.88(4)	2.06(4)	2.945(7)	176(7)	x, -1+y, z
N5	H6n	O20	0.88(6)	2.09(5)	2.949(8)	167(7)	½-x, ½+y, 1½-z
N7	H8n	O19	0.89(6)	2.20(6)	3.047(7)	161(6)	-x, 1-y, 1-z
N10	H10n	O13	0.88(3)	1.77(3)	2.646(6)	176(9)	x, y, z
N10	H11n	O6	0.88(5)	1.83(5)	2.700(7)	168(6)	½-x, ½+y, ½-z
N12	H12n	O14	0.88(6)	1.89(6)	2.765(8)	174(6)	x, y, z
N12	H13n	O1	0.88(2)	1.79(2)	2.656(6)	166(8)	½-x, ½+y, ½-z
N14	H14n	O2	0.88(3)	1.80(4)	2.681(7)	172(7)	½-x, ½+y, 1½-z
N14	H15n	O9	0.88(3)	1.77(4)	2.632(6)	168(7)	½-x, ½+y, 1½-z
N16	H16n	O10	0.88(5)	1.91(5)	2.766(7)	165(7)	x, y, z
N16	H17n	O5	0.88(3)	1.77(3)	2.628(6)	165(6)	-x, 1-y, 1-z

The eight constituents of the crystallographic asymmetric unit of **2**, Figures 2b-e and 3b-e, exhibit similar characteristics to those in **1**. A difference is evident in the anions in that these tend to be closer to co-planar in **2** compared with **1**, as seen in the range of dihedral angles between the carboxylate/nitro residues, which are 10-20° smaller than in **1**, Table 2. The key least-squares plane data for the anions in **1** and **2** generally lie within the ranges established for literature precedents of ammonium salts. The most planar anion is found in the ethylenediammonium dihydrate [12] for which the dihedral angles between the C6/CO_2, C6/NO_2 and CO_2/NO_2 pairs of planes are 3.44(14), 0.69(11) and 3.2(2)°. The greatest dihedral angle for C6/CO_2 of 26.4(3)° is found in the ammonium salt hydrate [6], C_6/NO_2 of 12.6(3)° in the di-*n*-butyl-ammonium salt [7] and CO_2/NO_2 of 26.73(14)° in the hydrazinium salt [9]. The differences between the anions in **1** and **2** are highlighted in the overlay diagram shown in Figure 4a. The cations are similar across the structures with one notable difference being in the dihedral angles formed between the best plane through the piperazin-1-ium ring and the acetyl residue, as highlighted in the overlay diagram of Figure 4b.

There is only one literature precedent for the 4-(4-acetylphenyl)piperazin-1-ium cation but, three-dimensional coordinates are not available [38].

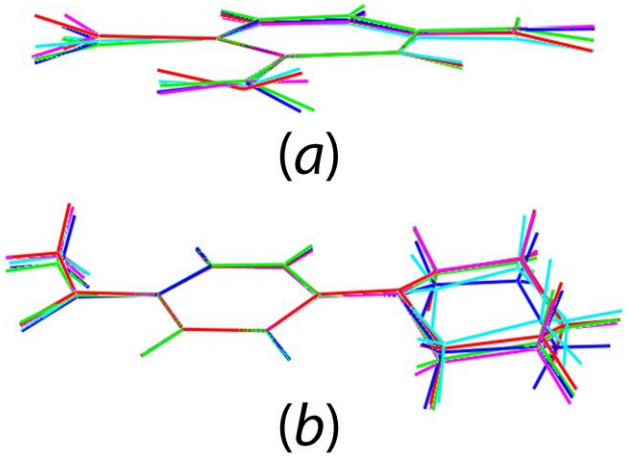

Fig. 4: Overlay diagrams of the ions in **1** and **2**: (**a**) anions in **1** (red image) and **2**, O1- (green), O5- (blue), O9- (aqua) and O13- (pink) containing anions and (**b**) cations in **1** (red image) and **2**, inverted-N10- (green), inverted-N12- (blue), N14- (aqua) and N16- (pink) containing cations. Anions and cations have been overlapped so the benzene rings are coincident in each of (**a**) and (**b**).

Molecular packing

Geometric parameters characterising the key interatomic interactions in the crystals of **1** and **2** are collated in Table 3. Hydrogen bonding features prominently in the molecular packing of both **1** and **2**, with each acidic N-bound hydrogen atom forming a N–H···O hydrogen bond.

In **1** and referring to Figure 5a, the intramolecular amine-N–H···O(carboxylate) hydrogen bond referred to above and which closes an S(6) ring is highlighted with a "1". The key supramolecular synthon in the structure is a centrosymmetric 12-membered {···HNH···OCO}$_2$ synthon is formed by charge-assisted ammonium-N–H···O(carboxylate) hydrogen bonds; the ring is indicated by a "2" and has a chair conformation. The remaining hydrogen bond occurs between like-ions, namely amine-N–H···O(nitro) and is marked with a "3" in Figure 5a; a significantly weaker amine-N–H···O(acetyl) hydrogen bond is also noted involving the amine-H atom

forming the intramolecular hydrogen bond. Consistent with the "charge-assisted" nature of the ammonium-N–H···O(carboxylate) hydrogen bonds, the N···O separations are systematically shorter than those of the other intermolecular N–H···O hydrogen bonds, Table 3. The result of the hydrogen bonding is the formation of double-layers in the bc-plane, Figure 5b. Additional stability to the double-layers is afforded by rather short methylene-C10–H10b···O1(carboxylate) and longer methylene-C9–H···O5(acetyl) interactions. Layers stack along the a-axis with the most prominent interactions between them being methylene-C10–H10a···O2(carboxylate), involving the second methylene-H10a bound to the C10 atom, and π-stacking interactions, the latter between the aromatic residues of anions and cations, Table 3 and Figure 5c.

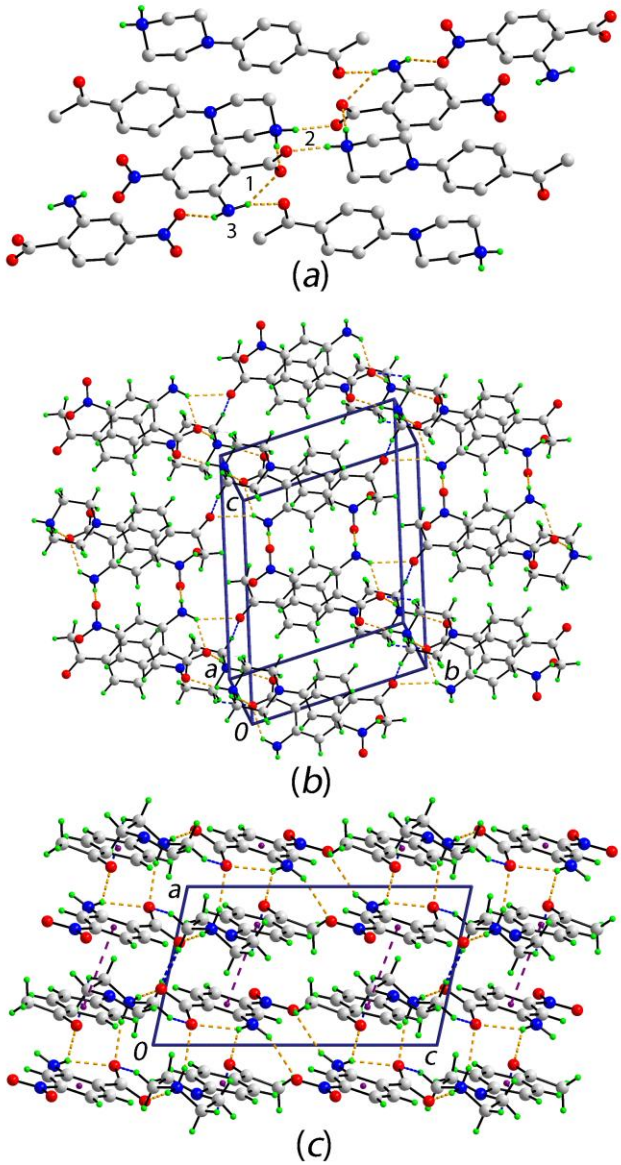

Fig. 5: Molecular packing in **1**: (**a**) detail of the N–H···O hydrogen bonding, shown as blue dashed lines, (**b**) supramolecular double-layer with C–H···O interactions shown as blue dashed lines and (**c**) a view of the unit cell contents in projection down the b-axis, with π···π stacking indicated by purple dashed lines.

The common feature of the molecular packing of **1** and **2**, the latter with four independent cations and anions, is the formation of charge-assisted ammonium-N–H···O(carboxylate) hydrogen bonds. However, unlike **1**, these strong hydrogen bonds give rise to highly-twisted supramolecular chains aligned along the c-axis, rather than cyclic synthons. The chains comprise all independent molecules in the asymmetric and features alternating cations and anions, Figure 6a. The connections between chains are of the type amine-N–H···O(carboxylate, acetyl) hydrogen bonds and these consolidate the three-dimensional packing, Figure 6b. Thus, the nature of the amine-N–H···O interactions also differ between **1** and **2** as in **1**, the main intermolecular amine-N–H···O hydrogen bond has a nitro-O atom as the acceptor whereas in **2**, the acceptors are carboxylate-O and acetyl-O atoms in the ratio 1:3. Other non-covalent interactions between the constituent ions are also found in the packing, e.g. C–H···O, C–H···N and π···π stacking. These are discussed in some detail in the section "Hirshfeld surface analysis".

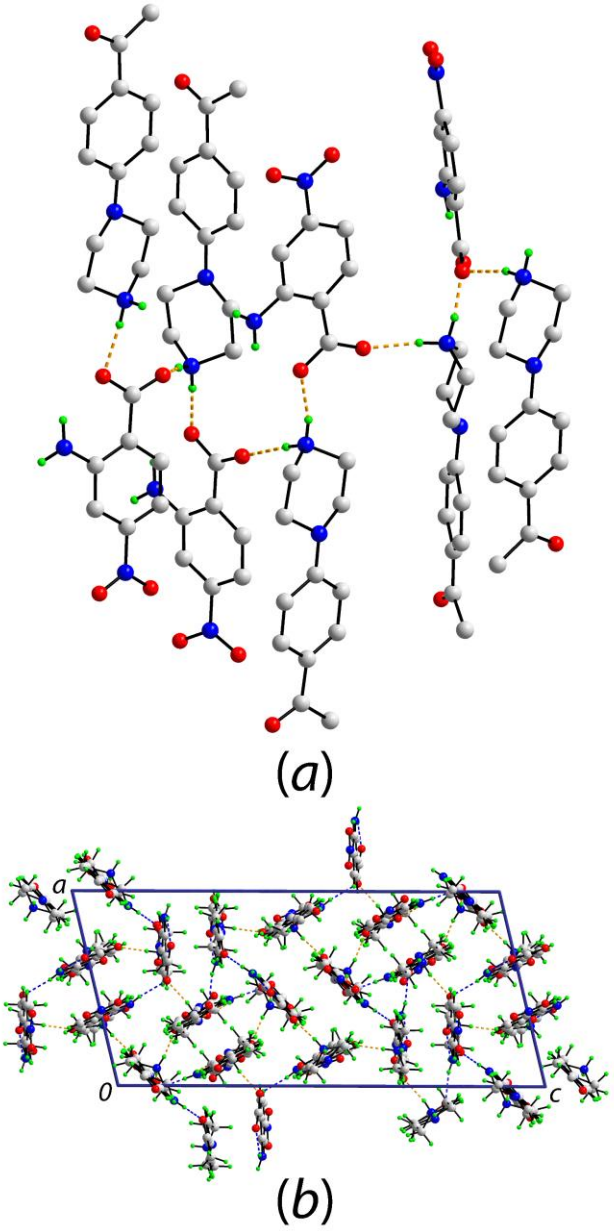

Fig. 6: Molecular packing in **2**: (**a**) view of the supramolecular chain along the *c*-axis of the unit cell sustained by charge-assisted ammonium-N–H···O(carboxylate)

hydrogen bonds shown as orange dashed lines; non-acidic hydrogen atoms are omitted and (**b**) view of the unit cell contents down the b-axis highlighting the connections between the chains of (a) by amine-N–H···O(carboxylate, acetyl) hydrogen bonds represented as blue dashed lines.

Hirshfeld surface analysis

The Hirshfeld surface calculations were carried out for the polymorphs **1** and **2** in accord with a recent study on an organic salt [39]. The results provide additional insight into the influence of non-covalent interactions on their molecular packing and assist in differentiating between the independent species found in **1** and **2**. Short interatomic contacts found in the crystals of **1** and **2** were as calculated in Crystal Explorer [30] and are listed in Table 4.

In the triclinic polymorph **1**, the amino-N1 atom forms a comparatively weak amino-N1–H···O5(acetyl) hydrogen bond whereas the amino-N1–H···O3(nitro) hydrogen bond is significantly shorter, Table 3: these result in diminutive and bright-red spots near the respective atoms on the Hirshfeld surfaces mapped over d_{norm} in Figure 7. The bright-red spots near the ammonium-H3n and H4n of the cation and the carbonyl-O1 and O2 atoms of the anion in Figure 7 also indicate charge-assisted N–H···O hydrogen bonds between the ions. The ions are also linked through methylene-C–H···O(carbonyl) and π···π contacts (Table 3) and short interatomic C···H contacts (Table 4). These are illustrated in Figure 8a-d and indicated by labels "1" – "4". The donors and acceptors of intermolecular interactions in the crystal are also viewed as the blue and red regions, respectively, on the Hirshfeld surfaces mapped over the calculated electrostatic potential shown in Figure 9. The influence of the other intermolecular C–H···O contacts (Table 3) appear as faint-red spots on the d_{norm}-mapped Hirshfeld surface (Figure 7) and are also highlighted with labels "5" – "8" in Figure 8a,c,d. In addition, the short interatomic contacts listed in Table 4 are also evident as faint-red spots near the respective atom in Figure 7.

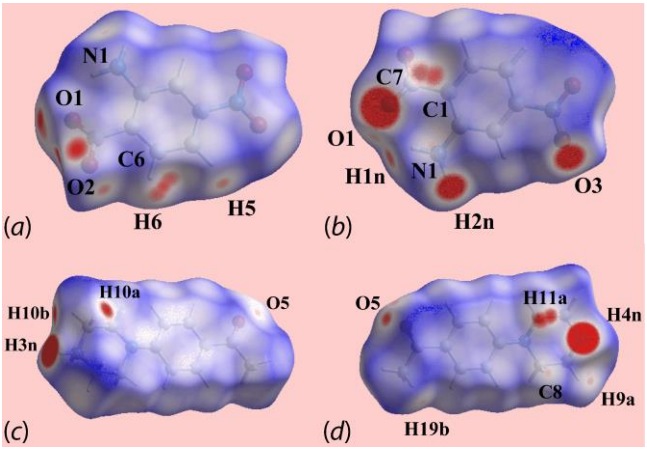

Fig. 7: Different views of the Hirshfeld surface mapped over d_{norm} in the range -0.205 to +1.598 atomic units (a.u.) for triclinic polymorph **1** for: (a) and (b) the anion, (c) and (d) the cation.

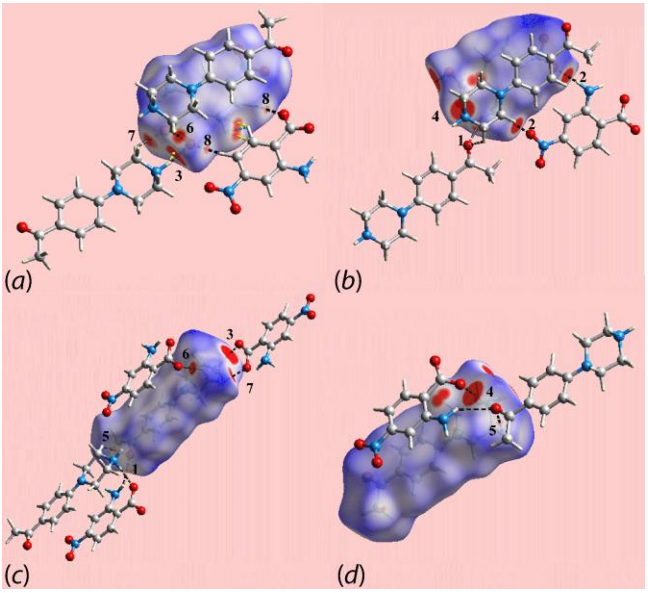

Fig. 8: Different views of the Hirshfeld surface mapped over d_{norm} in the range -0.205 to +1.598 a.u. for triclinic polymorph **1** highlighting the influence of the N–H···O and C–H···O interactions. See text for explanations of the labels "1" – "8".

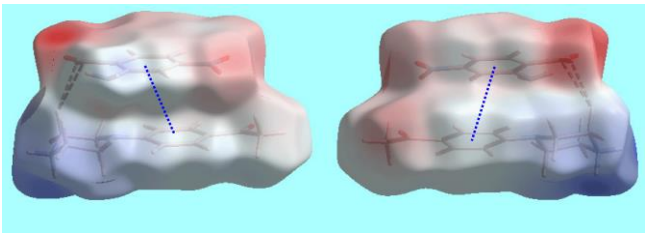

Fig. 9: Different views of the Hirshfeld surface mapped over the electrostatic potential in the range ±0.307 a.u. for triclinic polymorph **1**. The red and blue regions represent negative and positive electrostatic potentials, respectively. The intramolecular C···H/H···C and C–H···O contacts are highlighted with black dashed lines and π···π contacts with blue dotted lines.

Tab. 4: Summary of short inter atomic contacts (Å) in the crystals of **1** and **2**.

Contact	Distance	Symmetry operation
1		
H6···H6	2.01	1-x, 1-y, 2-z
C1···H11a	2.58	1+x, y, z
C6···H6	2.63	1-x, 1-y, 2-z
C7···H3n	2.44	1-x, -y, 2-z
C7···H10a	2.78	x, y, z
C7···H11a	2.58	1+x, y, z
N1···H8b	2.60	1+x, y, z
N1···H19b	2.60	1-x, -1-y, 1-z
O1···O5	2.97	1+x, -1+y, z
2		
H27···H41a	2.03	x, y, z
H29a···H66a	2.05	½+x. 1½-y, -½+z
H46···H64b	2.08	1-x, 1-y, 1-z
C1···C3	3.36	-x, 1-y, 1-z
C2···H38	2.78	½-x, -½+y, ½-z
C8···C71	3.30	½+x, ½-y, -½+z

C9···H56b	2.75	-x, 1-y, 1-z
C10···C69	3.35	½+x, ½-y, -½+z
C15···C59	3.37	x, y, z
C17···C57	3.36	x, y, z
C23···H68b	2.66	-x, 1-y, 1-z
C36···H30a	2.44	-x, 2-y, -z
C39···H30a	2.57	-x, 2-y, -z
C41···H27	2.76	x, y, z
C45···H27	2.69	x, y, z
C49···H26	2.71	x, y, z
C73···H53a	2.74	½-x, -½+y, 1½-z
C75···O5	3.12	-½+x, ½-y, ½+z
C63···O9	3.09	x, y, z
N3…H58	2.49	-x, 1-y, 1-z
N5···C32	3.22	½+x, 1½-y, ½+z
N5···H32a	2.57	½+x, 1½-y, ½+z
N7···H68b	2.48	-x, 1-y, 1-z
O16···H40a	2.54	x, -1+y, z
O1…H30b	2.55	½-x, -½+y, ½-z
O12…H64a	2.55	½-x, ½+y, 1½-z
O18…H7b6	2.57	½+x, ½-y, -½+z
O19…H24	2.45	-x, 1-y, 1-z

The similarities and differences in the supramolecular associations formed by each of the four cations and four anions in the asymmetric unit of the monoclinic polymorph with Z' = 4 can be conveniently delineated in their calculated Hirshfeld surfaces, see Figures 10-13. As there is no simple one-to-one association between any of the constituent cations and anions (Figure 13) in the crystal of monoclinic **2**, just as in case of triclinic **1** discussed earlier, distinctive charge-assisted ammonium-N–H···O(carboxy) and amino-N-H···O(carbonyl, nitro) hydrogen bonds are formed by each of the ions and result in characteristic features on the d_{norm}-mapped Hirshfeld surface shown in Figures 10 (anions) and 11 (cations). In addition, bright-red spots near the phenyl-C36, acetyl-C39 and methylene-H30a atoms in Figure 11a indicate the significant influence of short interatomic C···H contacts (Table 4) formed between symmetry-related N10-cations upon the crystal stability. The influence of a phenyl-C38–H···π(C1-C6) interaction, occurring between the N10-cation (Figure 11a) and O1-anion (Figure 10a), is also evident on the d_{norm}-mapped Hirshfeld surface and in the Hirshfeld surface mapped over the shape-index, Figure 13a (label "1"). The C33-C38 ring of the N10-cation also participates in a C–H···π interaction with the methylene-C65-H atom being the donor (Table 5), derived from the N16-cation, as shown in Figure 13b (label "2"). The phenyl-C26–H atom of the O13-anion also forms an intermolecular C–H···π contact with the C45-C50 ring of the N12-cation. The latter also participates in a π···π stacking interaction with a symmetry related ring as summarised in Table 5. These interactions are illustrated with labels "3" and "4" in Figure 13c. The acetyl-O18 atom, unlike the other equivalent atoms of the cations comprising **2**, does not act as an acceptor for an N–H···O hydrogen bond, rather it participates in a weak intermolecular methyl-C76–H...O18 interaction which is characterised as the faint-red spots near the respective atoms on the d_{norm}-mapped Hirshfeld surfaces of the respective cations in Figures 11b and d.

In the N14-cation, the acetyl-O19 atom is an acceptor for phenyl-C24–H···O as well as amino-N7–H···O interactions (Tables 3 and 4), with both of the respective donor atoms derived from the same O13-anion, Figure 12c. The atoms of the N14-cation are also involved in a π···π stacking and two C–H···π interactions. In one of the latter, methylene-C53–H atom forms a contact with a phenyl-(C69-C74) ring of the N16-cation, while in the other, the methylene-C41–H and phenyl-(C57-C62) ring act as a donor and acceptor, respectively (Figure 13d, labels "5" and "6"). The

presence of bright-red spots viewed near the phenyl-C58–H58 atom in Figure 11c also reflects the influence of the C58–H···N3 interaction with the amino-N3 atom of the O5-anion (Table 4). A π···π contact between the phenyl-(C57-C62) ring of the N14-cation and the phenyl-(C15-C20) ring of the O9-anion is highlighted in Figure 13e with label "7". The weak intermolecular C–H···N interactions formed between the methylene-C32–H atom of the N10-cation and amino-N5 atom of the O9-anion, and between the methylene-C68-H atom of the N16-cation and the amino-N7 atom of O13-anion results in faint-red spots near the respective atoms on their Hirshfeld surface (Figures 10c and d; Figures 11a and d).

The aromatic residues of anions are also involved in intermolecular π···π and N–O···π contacts (Table 5). The phenyl-(C1-C6) ring of the O1-anion forms a π···π contact with an inversion-related ring (Figure 13a with label "8") while the nitro-O4 atom of the O5-anion forms a N–O···π contact with the phenyl-(C15-C20) ring of the O9-anion (Figure 13f with label "9"). Another N–O···π interaction is noted, involving the nitro-O16 atom of the O13-anion with the phenyl-(C22-C27) ring of an inversion related O13-anion (Figure 13g with label "10"). Finally, a π···π contact between phenyl-(C8-C13) of the O5-anion and phenyl-(C69-C74) rings of the N16-cation are highlighted with label "11" in Figure 13h. The influence of other short interatomic contacts summarised in Table 4 for the mono-clinic polymorph are reflected as the faint-red spots near the respective atoms on their d_{norm}-mapped Hirshfeld surfaces shown in Figures 10 and 11.

The overall two-dimensional fingerprint plots for polymorphs **1** and **2**, and those delineated into H···H, O···H/H···O, C···H/H···C and C···C contacts [31], are illustrated in Figure 14. The percentage contributions from the different interatomic contacts to their respective Hirshfeld surfaces for the overall salt, and individual anions and cations are summarized in Table 6.

In triclinic **1**, the short interatomic H···H contact involving symmetry-related phenyl-C–H6 atoms of the anion (Table 4) appears as the parabolic distribution of points with the broad peak at $d_e + d_i \sim 2.0$ Å in the fingerprint delineated into H···H contacts (Figure 14a). The well-defined two pairs of overlapping spikes at $d_e + d_i \sim 1.9$ Å in the fingerprint delineated into O···H/H···O contacts are due to the charge-assisted N–H···O hydrogen bonds between cations and anions. The points corresponding to other intermolecular N–H···O and C–H···O interactions at greater $d_e + d_i$ distances are merged within the plots in Figure 14a. The π···π contact between aromatic rings of the cation and anion resulted greater, i.e. 8.3 and 6.1% contributions, respectively, from C···C contacts to their respective individual Hirshfeld surfaces, but the value decreases to 3.8% for the overall salt as some of these contacts occur between ions within the asymmetric unit (Table 6 and Figure 14a). The notable percentage contributions from C···H/H···C and N···H/H···N contacts to the Hirshfeld surfaces of the ions are due to the short interatomic contacts formed by their respective atoms (Table 4).

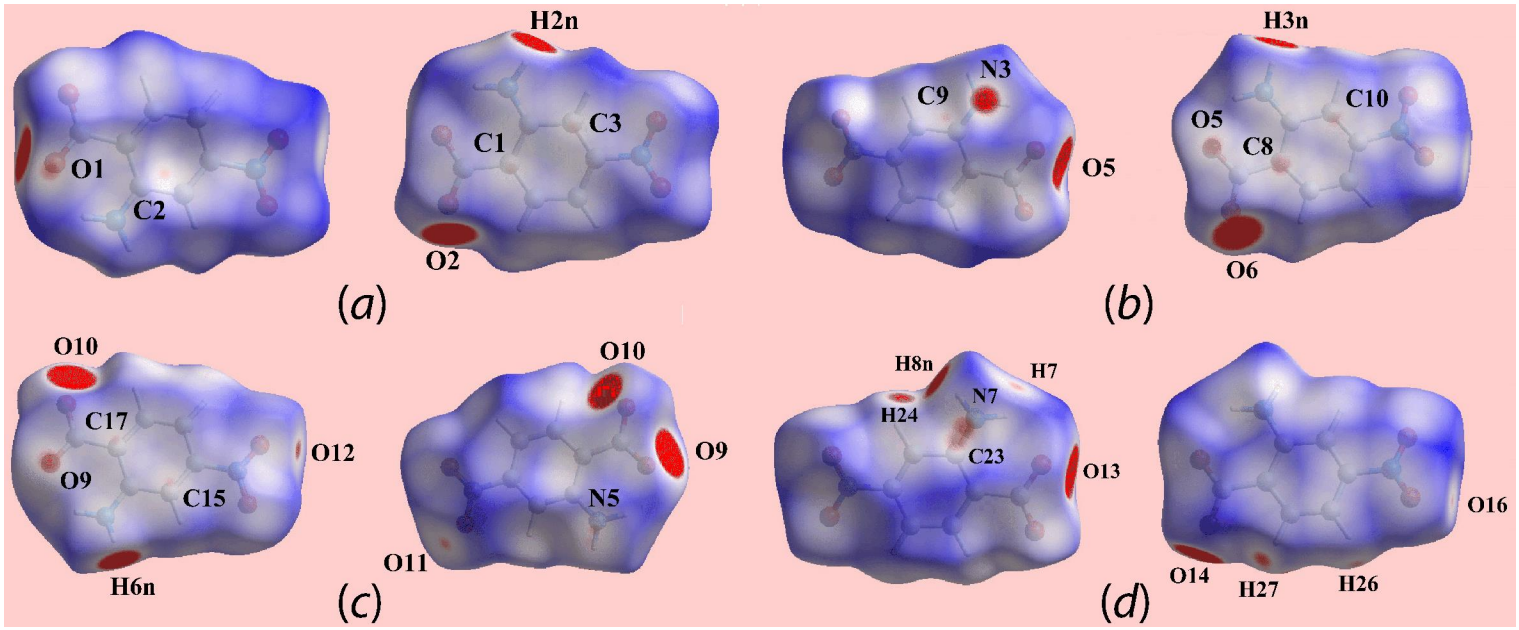

Fig. 10: Different views of the Hirshfeld surface mapped over d_{norm} in the range -0.155 to +1.591 a.u. for the (**a**) O1-, (**b**) O5-, (**c**) O11- and (**d**) O15-anions of monoclinic polymorph **2**.

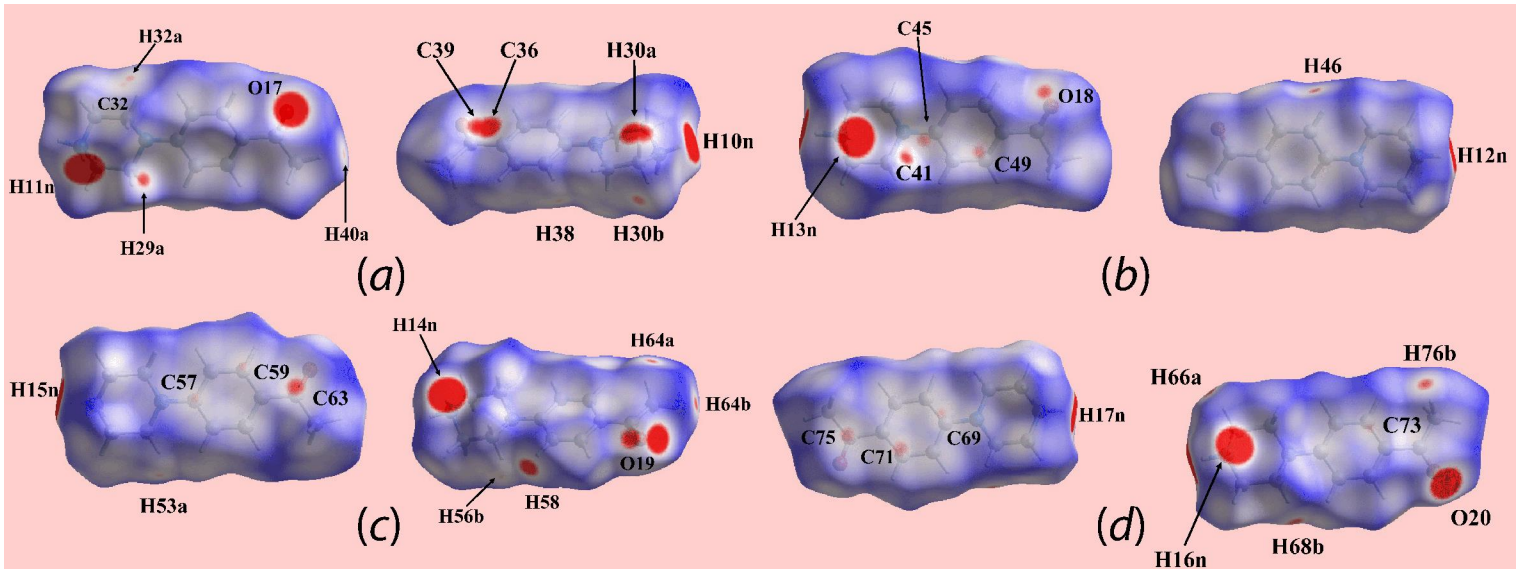

Fig. 11: Different views of the Hirshfeld surface mapped over d_{norm} in the range -0.155 to +1.591 a.u. for the (**a**) N10-, (**b**) N12-, (**c**) N14- and (**d**) N16-cations of monoclinic polymorph **2**.

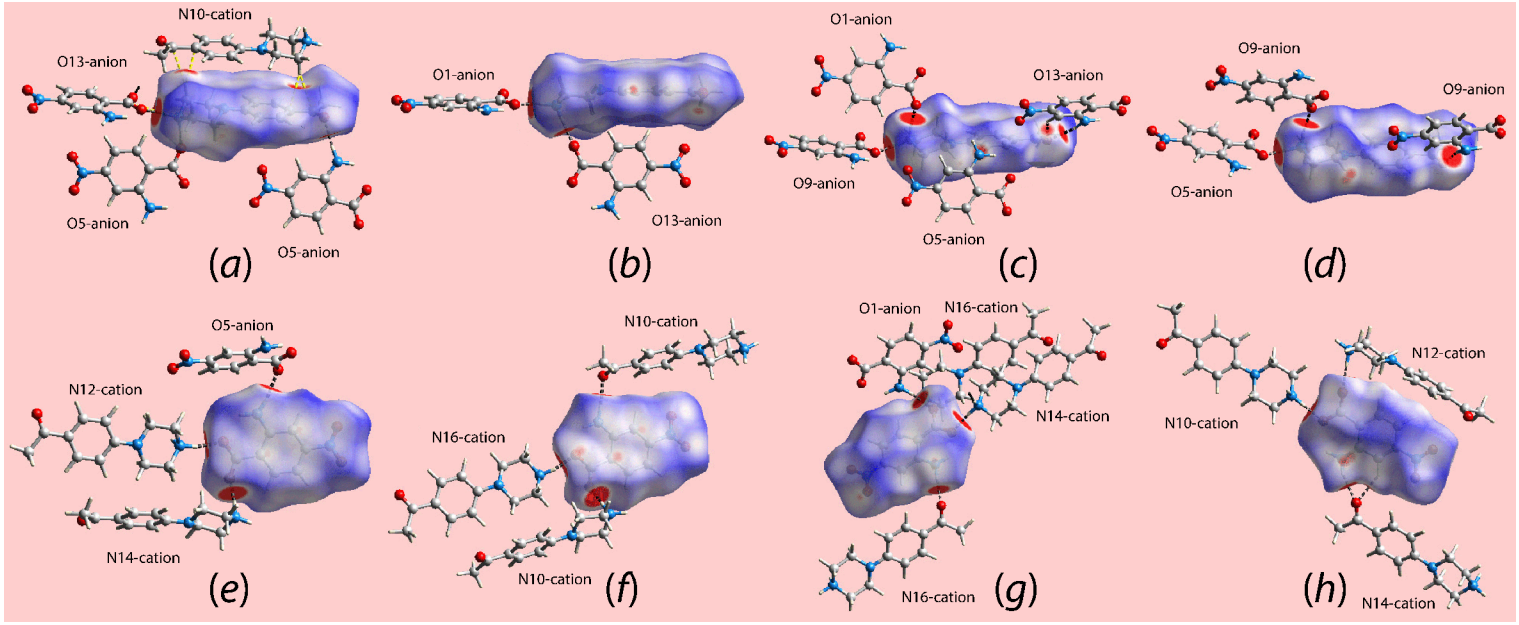

Fig. 12: Different views of the Hirshfeld surface mapped over d_{norm} in the range -0.155 to +1.591 a.u. for the (**a**)-(**d**) N10-, N12-, N14 and N16-cations, respectively, and (**e**)-(**h**) O1-, O5-, O9- and O13-anions, respectively, in monoclinic polymorph **2**, highlighting the immediate environments of the different constituent ions forming intermolecular N–H...O and C–H...O interactions.

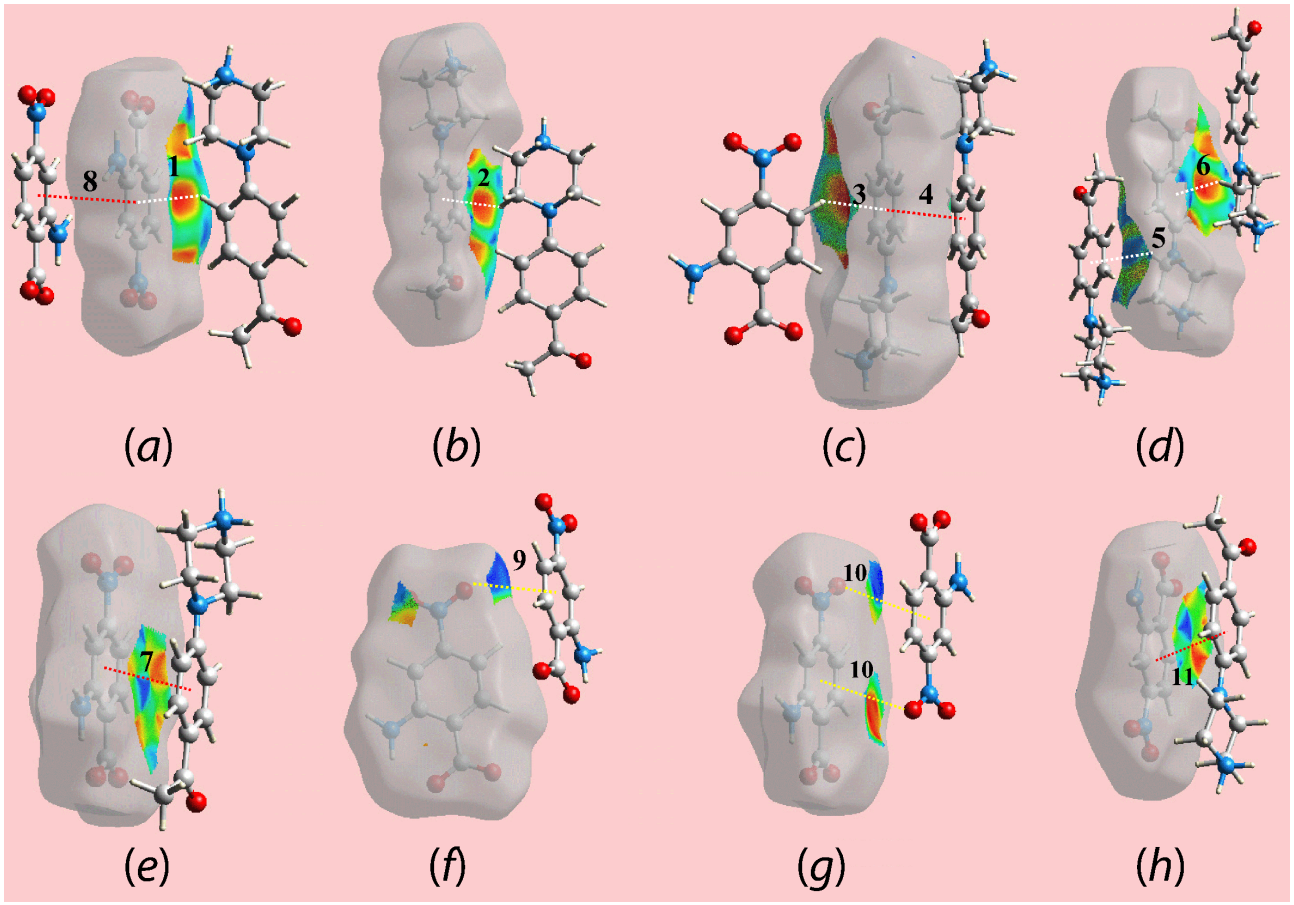

Fig. 13: (**a**)-(**h**) Views of the Hirshfeld surfaces mapped with shape-indexed properties for the monoclinic polymorph **2**, highlighting C–H...π, N–O...π and π–π stacking interactions between the constituent ions as white, yellow and red dotted lines, respectively. For a detailed discussion of the distances labelled as "1" to "11", please refer to the explanation in the main text.

The fingerprint plots delineated into H···H contacts for the overall monoclinic polymorph **2** characterise these short interatomic contacts as summarised in Table 4 and Figure 14b. They are viewed as a pair of very short and close tips at $d_e + d_i \sim 2.1$ Å in the delineated plot. In the fingerprint plot delineated into O···H/H···O contacts, the pair long spikes with tips at $d_e + d_i \sim 1.8$ Å in the donor and the acceptor regions have a greater density of points as a result of the charge-assisted N–H···O hydrogen bonds. The short spike with the tip at $d_e + d_i \sim 2.5$ Å is indicative of the C–H···O contact involving the acetyl-O18 atom (Table 4) and those corresponding to the other intermolecular C–H···O contacts are merged within the plot. It is evident from the fingerprint plots delineated into C···H/H···C contacts for polymorphs **1** and **2** and the percentage contributions to their Hirshfeld surfaces (Table 6) that these interactions have a greater influence upon the packing in monoclinic **2** compared with triclinic **1**, arising from the greater number of C···H/H···C and C–H···π interactions in **2** in contrast to only a few comparable contacts in **1**, as can be seen from the data in Table 4. Conversely, the percentage contributions of H···H contacts to the Hirshfeld surface in **2** is less than that in **1**.

The π···π stacking interactions occurring between the aromatic rings of polymorph **2** (Table 5) give rise to a notable contribution from C···C contacts to the Hirshfeld surface. The small contribution from these contacts to the Hirshfeld surface of the individual O13-anion and N10-cation (Table 6) indicate their non-participation in such interactions and distinguish these species from the other anions/cations comprising the asymmetric unit. Although making a smaller, i.e. 2.8%, contribution to the Hirshfeld surface compared with 3.8% in triclinic form **1**, π···π stacking interactions in **2** are also indicated in the C···C delineated fingerprint plot (Figure. 14b). The relatively small percentage contributions from C···O/O···C contacts to the Hirshfeld surfaces of the anions (Table 6) reflect the presence of short interatomic C···O/O···C contacts (Table 4) and N–O···π contacts (Table 5) involving aromatic rings of the O9- and O13-anions as acceptors. The smaller contributions of the other interatomic contacts summarised in Table 6 have a negligible impact on the packing.

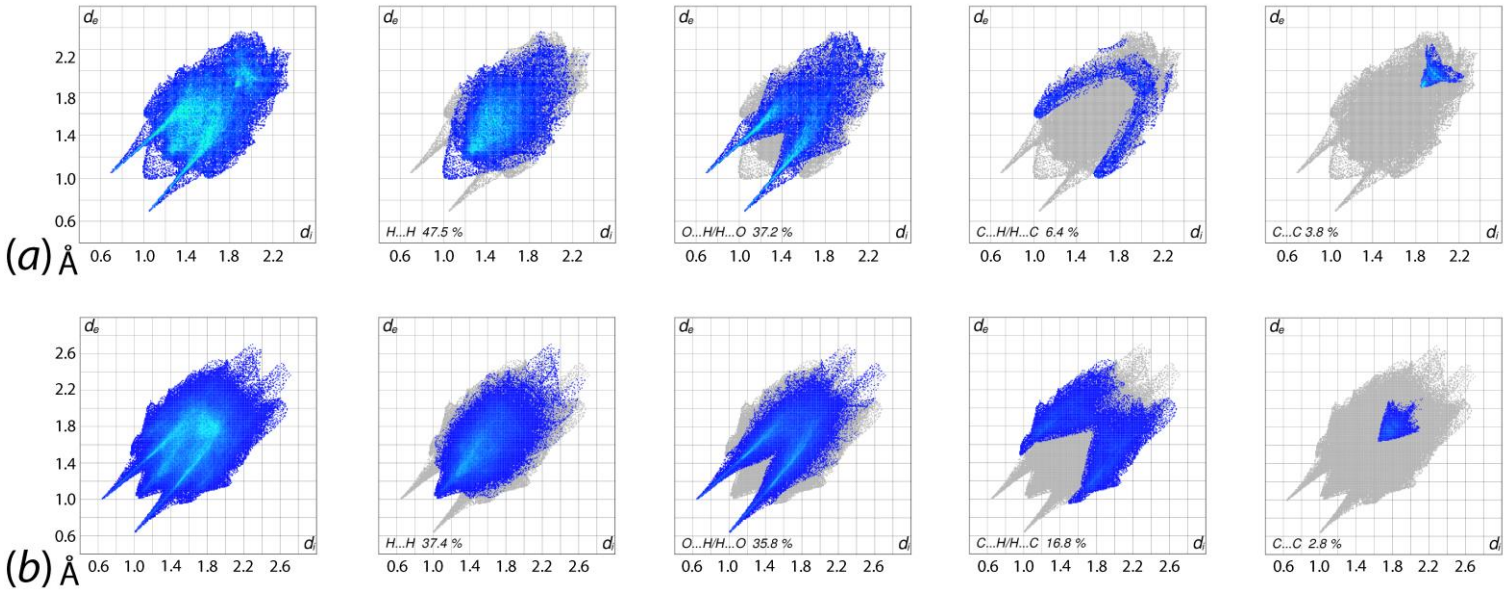

Fig. 14: The overall two-dimensional fingerprint plot and those delineated into H···H, O···H/H···O, C···H/H···C and C···C contacts for (a) triclinic polymorph **1** and (b) monoclinic polymorph **2**.

Tab. 5: Summary of C–H···π , N–O···π and π···π interactions (Å, °) in the crystal of monoclinic polymorph **2**.

A	H	B	A–H···B	H···B	A···B	A–H…B	Symmetry operation
C26	H26	Cg(C45-C50)	0.95	2.63	3.442(8)	144	x, y, z
C38	H38	Cg(C1-C6)	0.95	2.78	3.633(7)	151	½-x, ½+y, ½-z
C41	H41b	Cg(C57-C62)	0.99	2.72	3.619(8)	152	x, y, -1+z
C53	H53a	Cg(C69-C74)	0.99	2.87	3.683(7)	139	½-x, ½+y, 1½-z
C65	H65a	Cg(C33-C38)	0.99	2.73	3.577(8)	143	-½+x, 1½-y, ½+z

N2	O4	Cg(C15-C20)	1.212(9)	3.851(8)	4.777(8)	134.3(5)	x, y, z
N8	O16	Cg(C22-C27)	1.228(7)	3.740(6)	4.069(6)	96.6(4)	-x, 1-y, -z
Cg(C1-C6)	-	Cg(C1-C6)	-	-	3.651(4)	-	-x, 1-y, 1-z
Cg(C8-C13)	-	Cg(C69-C74)	-	-	3.489(4)	-	½+x, ½-y, -½+z
Cg(C15-C20)	-	Cg(C57-C62)	-	-	3.620(3)	-	x, y, z
Cg(C45-C50)	-	Cg(C45-C50)	-	-	3.606(4)	-	1-x, 1-y, -z

Tab. 6: Percentage contributions from the different intermolecular contacts to the Hirshfeld surfaces of triclinic polymorph **1**, monoclinic polymorph **2** and for the individual anions and cations in each of **1** and **2**.

Contact	**1**	**2**	anion in **1**	O1-anion in **2**	O5-anion in **2**	O9-anion in **2**	O13-anion in **2**	cation in **1**	N10-cation in **2**	N12-cation in **2**	N14-cation in **2**	N16-cation in **2**
H···H	47.5	37.4	27.8	23.3	25.2	23.6	20.3	50.2	44.6	45.4	43.5	44.4
O···H/H···O	37.2	35.8	44.2	41.0	46.0	44.4	45.8	29.1	27.4	31.2	30.8	31.1
C···H/H···C	6.4	16.8	9.7	19.1	13.8	15.7	21.0	7.3	22.2	15.6	16.8	15.3
N···H/H···N	0.9	3.2	3.0	3.0	3.2	4.5	4.3	1.7	3.4	2.0	2.9	1.9
C···C	3.8	2.8	8.3	4.7	5.6	4.7	1.5	6.1	0.4	3.2	3.5	4.2
C···O/O···C	1.8	1.7	2.5	3.2	3.4	5.1	5.8	2.2	0.3	0.7	1.1	1.1
C···N/N···C	1.3	1.1	3.6	1.5	1.4	0.6	0.9	2.6	1.3	1.0	0.5	1.1
O···O	1.1	0.7	0.9	2.8	0.7	0.5	0.4	0.9	0.4	0.3	0.4	0.5
N···O/O···N	0.0	0.3	0.0	1.5	0.0	0.6	0.0	0.0	0.0	0.6	0.3	0.0
N···N	0.0	0.2	0.0	0.0	0.7	0.2	0.0	0.0	0.0	0.0	0.2	0.5

A comparison between polymorphic forms 1 and 2

A summary is presented in Table 7 of some of the key physiochemical properties for **1**, **2** and their components which were calculated with Crystal Explorer [30] and PLATON [28]. Some noteworthy differences in the parameters describing the anions in each of **1** and **2** are clearly apparent from these data. Thus, the volume (V) occupied by the anion in **1** is smaller by up to 10 $Å^3$ compared with to the comparable volumes for each of the anions in **2**. This correlates with an increase in the surface areas (A) in **2** compared with **1**, so that the A:V ratio remains approximately the same. Except for the globularity value (G) of 0.829 calculated for the O13-anion, these values are constant across the series. Finally, the value for asphericity (Ω) for the anion in **1** lies within the range for those calculated for **2**. There are no apparent systematic variations in the values of V, A and Ω for the cations in **1** and **2**. The value of G in **1** appears to be higher than the comparable values in **2** but, the differences are small.

A comparison between **1** and **2** is also made in Table 7 in terms of the density and overall packing efficiency. The greater density of **1** correlates with its greater packing efficiency when compared to that of **2**. The approximate packing energies for **1** and **2** were also calculated using empirical potential parameters [40], as implemented in Mercury [41]. The values, Table 7, are in accord with the trends above in that they suggest the triclinic form **1** is the more stable of the polymorphs, consistent with this being the thermodynamic form.

Tab. 7: Physiochemical properties for **1** and **2**.

Property	**1**	**2**	**1** – anion	**2** – O1-anion	**2** – O5-anion	**2** – O9-anion	**2** – O13-anion	**1** – cation	**2** – N10-cation	**2** – N12-cation	**2** – N14-cation	**2** – N16-cation
Volume, V ($Å^3$)	888.66(13)	7267.0(19)	173.31	184.05	181.54	182.47	184.78	261.02	258.27	269.38	258.56	257.16
Surface area, A ($Å^2$)			183.39	190.75	188.81	189.07	189.21	250.85	253.63	257.97	251.31	249.94
A:V ($Å^{-1}$)			1.06	1.04	1.04	1.04	1.04	0.97	0.98	0.96	0.97	0.97
Globularity, *G*			0.820	0.820	0.821	0.823	0.829	0.787	0.773	0.782	0.781	0.782
Asphericity, Ω			0.165	0.173	0.169	0.162	0.157	0.305	0.309	0.303	0.301	0.312
Density (g cm^{-1})	1.444	1.413										
Packing index (%)	73.8	71.8										
Packing energy (kJ mol^{-1})	-282.5	-257.9										

Conclusions

X-ray crystallography has been employed to characterise two salts, a monoclinic form, with Z' = 4, which was isolated directly from the reaction mixture is, based on several criteria, including packing efficiencies and calculated lattice energies, likely to be a kinetic outcome of crystallisation. A re-crystallisation over a week afforded a triclinic form, with Z' = 1, which is likely a thermodynamically more stable form. Hirshfeld surface analyses proved a convenient manner by which the different constituent ions, in and within the polymorphs, could be differentiated in terms of their intermolecular interactions.

Acknowledgements: The use of the NCS crystallographic service at the University of Southampton, UK, and the valuable assistance of the staff there are gratefully acknowledged. JLW thanks FAPERJ and CNPq, Brazil, for support. Sunway University is also thanked for support of research into co-crystallisation experiments through Grant No. INT-RRO-2016-060.

References

[1] J. L. Wardell, E. R. T. Tiekink, *J. Chem. Cryst*. **2011**, *41*, 1418.
[2] S. M. S. V. Wardell, J. L. Wardell, *J. Chem. Cryst*. **2016**, *46*, 34.
[3] G. Smith, *Acta Crystallogr. C* **2013**, *69*, 1472.
[4] G. Smith, *Acta Crystallogr. E* **2014**, *70*, m192.
[5] G. Smith, *Acta Crystallogr. E* **2011**, *67*, m1047.
[6] G. Smith, Private Communication to the CSD, **2014**. Refcode DOBPIV.
[7] J. L. Wardell, M. M. Jotani, E. R. T. Tiekink, *Acta Crystallogr. E* **2016**, *72*, 1691.
[8] G. Smith, U. D. Wermuth, P. C. Healy, *Acta Crystallogr. E* **2004**, *60*, o684.
[9] J. L. Wardell, M. M. Jotani, E. R. T. Tiekink, *Acta Crystallogr. E* **2017**, *73*, 579.
[10] G. Smith, D. E. Lynch, *Acta Crystallogr. C* **2016**, *72*, 105.
[11] G. Smith, U. D. Wermuth, P. C. Healy, J. M. White, *Acta Crystallogr. E* **2007**, *63*, o7.
[12] G. Smith, U. D. Wermuth, J. M. White, *Acta Crystallogr. E* **2002**, *58*, o1088.
[13] H.-L. Chen, C.-F. Huang, *Synth. React. Inorg., Met.-Org., Nano-Met. Chem*. **2009**, *39*, 533.
[14] A. J. Cruz-Cabeza, S. M. Reutzel-Edens, J. Bernstein, *Chem. Soc. Rev.* **2015**, *44*, 8619.
[15] S. L. Price, *Acc. Chem. Res*. **2009**, *42*, 117.
[16] C. R. Groom, I. J. Bruno, M. P. Lightfoot, S. C. Ward, *Acta Crystallogr. B* **2016**, *72*, 171.
[17] K. Kersten, R. Kaur, A. Matzger, *IUCrJ* **2018**, *5*, 124.
[18] W. C. McCrone, in: D. Fox, M. M. Labes, and A. Weissberger (Eds.), Physics and Chemistry of the Solid State. Vol. 2. Wiley Interscience, pp. 725, **1965**.
[19] M. B. Hickey, M. L. Peterson, L. A. Scoppettuolo, S. L. Morrisette, A. Vetter, H. Guzmán, J. F. Remenar, Z. Zang, M. D. Tawa, S. Haley, M. J. Zaworotko, Ö. Almarsson, *Eur. J. Pharm. Biopharm*. **2007**, *67*, 112.
[20] W. W. Porter, S. C. Elie, A. J. Matzger, *Cryst. Growth Des*. **2008**, *8*, 14.
[21] Steed, K. M., Steed, J. W. *Chem. Rev*. **2015**, *115*, 2895.
[22] C. P. Brock, *Acta Crystallogr. B* **2016**, *72*, 807.
[23] J. W. Steed, *CrystEngComm*, **2003**, *5*, 169.
[24] V. S. Senthil Kumar, A. Addlagatta, A. Nangia, W. T. Robinson, C. K. Broder, R. Mondal, I. R. Evans, J. A. K. Howard, F. H. Allen, *Angew. Chem. Int. Ed*. **2002**, *41*, 3848.
[25] K. M. Anderson, M. R. Probert, C. N. Whiteley, A. M. Rowland, A. E. Goeta, J. W. Steed, *Cryst. Growth Des*. **2009**, *9*, 1082.
[26] C. P. Brock, J.D. Dunitz, J. D. *Chem. Mater*. **1994**, *6*, 1118.
[27] K. M. Anderson, A. E. Goeta, J. W. Steed, *Cryst. Growth Des.* **2008**, *8*, 2517.
[28] A. L. Spek, *J. Appl. Crystallogr*. **2003**, *36*, 7.
[29] J. J. McKinnon, M. A. Spackman, A. S. Mitchell, *Acta Crystallogr. B* **2004**, *60*, 627.
[30] S. K. Wolff, D. J. Grimwood, J. J. McKinnon, M. J. Turner, D. Jayatilaka, M. A. Spackman, Crystal Explorer (Version 3.1), University of Western Australia, **2012**.

[31] J. J. McKinnon, D. Jayatilaka, M. A. Spackman, *Chem. Commun*. **2007**, p. 3814.
[32] CrystalClear-SM Expert. User Manual. Rigaku/MSC Inc., Rigaku Corporation, The Woodlands, TX, **2011**.
[33] G. M. Sheldrick, *Acta Crystallogr. A* **2008**, *64*, 112
[34] G. M. Sheldrick, *Acta Crystallogr. C* **2015**, *71*, 3.
[35] L. J. Farrugia, *J. Appl. Crystallogr*. **2012**, *45*, 849.
[36] DIAMOND, Visual Crystal Structure Information System, Version 3.1, CRYSTAL IMPACT, Postfach 1251, D-53002, **2006**.
[37] J. Gans, D. Shalloway, *J. Mol. Graph. Model*. **2001**, *19*, 557.
[38] J. N. Gamlin, G. Olovsson, K. Pitchumani, V. Ramamurthy, J. R. Scheffer, J. Trotter, *Tetrahedron Lett*. **1996**, *37*, 6037.
[39] M. M. Jotani, J. L. Wardell, E. R. T. Tiekink, *Z. Kristallogr.* 2016, **231**, 247.
[40] A. Gavezzotti, *Acc. Chem. Res*. **1994**, *27*, 309.
[41] I. J. Bruno, J. C. Cole, P. R. Edgington, M. Kessler, C. F. Macrae, P. McCabe, J. Pearson, R. Taylor, *Acta Crystallogr. B* **2002**, *58*, 389.